Silicon Photonic Delay-Based Reservoir Computing Incorporated with a Multimode Interference Structure

Takashi Kan(1), Shota Ishimura(1), Hideaki Tanaka(1), Hidenori Takahashi(1), Takehiro Tsuritani(1), Katsuyuki Utaka(2), and Masatoshi Suzuki(1,2)

(1) KDDI Research, Inc., tk-kan@kddi.com
(2) Department of Electronic and Physical Systems, Waseda University

Abstract *We propose and experimentally demonstrate delayed-feedback type reservoir computing with a multimode interference structure in a silicon photonics. By combining both temporal and spatial nodes, the total number of nodes is increased to 1100, and the accuracy for the time series prediction is greatly improved. ©2023 The Author(s)*

Introduction

Due to the rapid evolution of artificial intelligence (AI) technologies such as neural networks (NNs), the significant increase in power consumption has become a rising concern since NNs consume considerable computational energy [1,2]. This issue could potentially be avoided by using photonics-based approaches with their lower power consumption than conventional electrical-based approaches [2-5]. Among the photonic approaches, reservoir computing (RC) has attracted significant attention due to its simpler architecture [3-20]. In addition, RC with a delayed feedback scheme [6,7] can potentially speed up the system because high-speed optical telecom devices can be used [15]. Thus far, numerous demonstrations of delay-based RC have been shown using bulky optical components [6,8-11,13-16].

On the other hand, photonic RCs implemented using integration technologies, such as silicon photonics, provide miniaturization and mass productivity [12,18-20]. However, integrated RC with delayed feedback scheme has not been demonstrated in silicon photonics because increasing nodes requires a long delay line, usually several hundred metres [14] or even more, which is difficult to achieve in integrated platforms. Recently, a new type of photonic integrated RC using multimode interference (MMI) has been proposed, where complex interference of guided modes in a multimode waveguide (MMW) ensures rich connections among spatial nodes [19,20]. In addition, the modal dispersion inside the MMW also provides fading memory [19]. By using this MMI-based architecture, the number of nodes can be expanded up to 260 by simultaneously exploiting 65 spatial nodes and four temporal nodes, this node expansion is 5.2 times larger than a silicon photonic RC chip reported in [18]. However, a further increase in the number of nodes of the MMW-based architecture may face technical difficulties due to the following perspectives: First, although the increase in the MMW width simply leads to an increase in the number of spatial nodes, it also leads to power density reduction, degrading the signal-to-noise ratio (SNR) at each spatial port. Another approach to increase the number of nodes is increasing temporal nodes using group delay differences among spatial modes, but modal dispersion is simply limited by the waveguide length. In fact, the RC reported in [19] achieved only a 200-ps delay with the 39 mm-long MMW. Since a longer MMW significantly increases the device size, it is difficult to further scale.

In this work, we experimentally demonstrate further node expansion by introducing an MMI-based architecture into the delay-based scheme; this, is the first demonstration of a delayed feedback RC in silicon photonics. For a delay-based RC, a ring length of 1.29 cm supports 11 temporal nodes in the our demonstration. By multiplying temporal nodes with the 100 spatial nodes of the following MMW, the number of nodes is increased to 1100 which is 4.2 times larger than that reported in ref. [19]. As a result, a normalized mean square error (NMSE) of 0.0107, which is smaller than the value reported so far experimentally, was obtained for the Santa Fe time series one-step prediction task.

Device design and characterization

Figure 1(a) shows the schematic concept of our RC chip. It consists of 2 sections: a ring cavity of a single mode waveguide (SMW) and a bending MMW. For the ring section, we designed the delayed feedback based on the asynchronous configuration as introduced in [9]; specifically, when the loop roundtrip time is T, the period of the input signal T' is given as $T' = TN_v / (N_v + 1)$, where N_v is the number of temporal nodes [14]. Here, denoting the duration per temporal node as θ, T and T' are given as $T = (N_v + 1)\theta$ and $T' = N_v\theta$, respectively. For the MMW section, we used

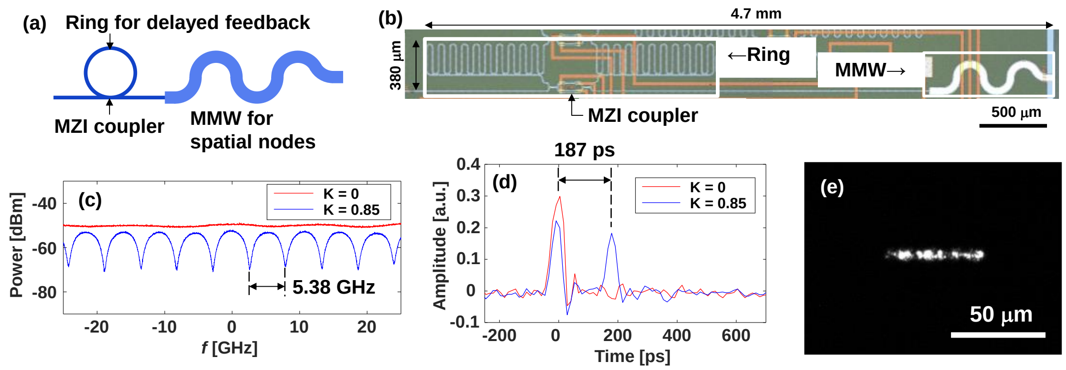

Fig. 1: Device design and characterization: (a) schematic configuration of the chip, (b) micrograph of the fabricated chip, (c) transmission of the ring, (d) pulse response of the ring, (e) near-field pattern of the MMW output.

a snake-crawling-shaped structure to cause more complex interference between guided modes. The details of the device design are described in our previous study [20]. The waveguide width of the MMW is set to 50 µm, which supports 126 guided transverse electric (TE) modes, to accommodate more than 100 modes while keeping the reduction in power density within acceptable levels.

Figure 1(b) shows the fabricated chip designed based on the above concept. It was fabricated on a standard silicon-on-insulator wafer with a 220-nm-thick silicon layer and SiO_2 cladding. The ring was designed based on an SMW with a 440-nm width. We set the aforementioned parameters as N_v = 11, θ = 15.59 ps, and thus T = 187 ps. To achieve this T value, the ring length was set to 1.29 cm. The SMW and ring were coupled via a tuneable Mach-Zehnder interferometer (MZI) coupler [21]. Two heaters were formed on the top of the MZI arms to control the SMW-to-ring coupling ratio, K. The ring section was designed using a hairpin-turned structure, as shown in Fig. 1(b); however, it could also be made using a swirl-shaped structure for further footprint reduction. Figures 1(c) and (d) show the transmission spectra and temporal output waveforms for the pulse input when the tuning powers applied to the heater were 24 and 12 mW, respectively. In these figures, the corresponding K values were estimated to be 0 and 0.85, respectively. For K = 0, there was no coupling to the ring; thus, a flat spectrum and no delayed response were observed. For K = 0.85, periodic dips with a free spectral range (FSR) of 5.38 GHz were observed, as shown in Fig. 1(c). The time interval between the two peaks in Fig. 1(d) was measured to be 187 ps, which was in good agreement with the designed ring roundtrip time T and the corresponding FSR.

For the MMW, the bending radius and total length of the MMW section were 100 µm and ~1.3 mm, respectively [20]. Figure 1(e) shows the near-field pattern of the MMW output at a wavelength of 1550 nm and a temperature of 20.6 °C; guided speckle light was distributed over the entire waveguide width.

Experimental setup

Figure 2 shows the experimental setup. Input masking was applied to the input signal $u(n)$ with offline digital signal processing (DSP) [7], and then the processed signal was sent to an arbitrary waveform generator (AWG). As a masking pattern, we used a uniformly distributed random sequence. The masked signal was then output from the AWG operating at 64.16 Gsample/s (= $1/\theta$) and was supplied to a $LiNbO_3$ intensity modulator (V_π = 3.07 V at DC) to modulate the output light from the continuous wave laser with a linewidth of 100 kHz at 1550 nm. The output

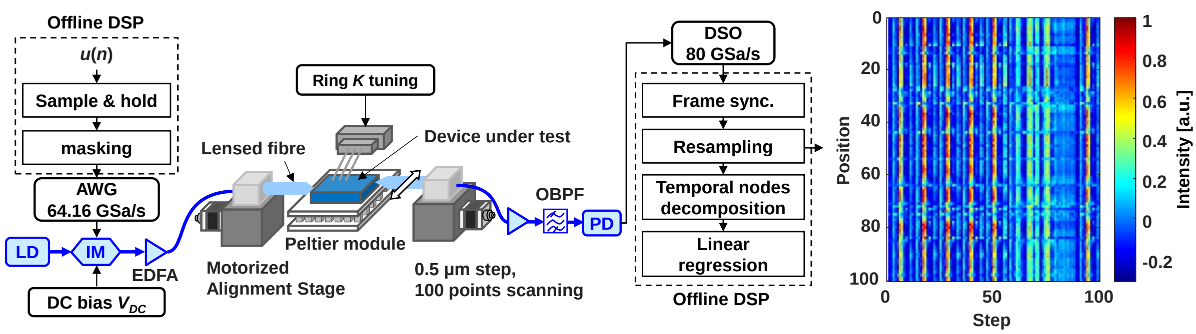

Fig. 2: Experimental setup.

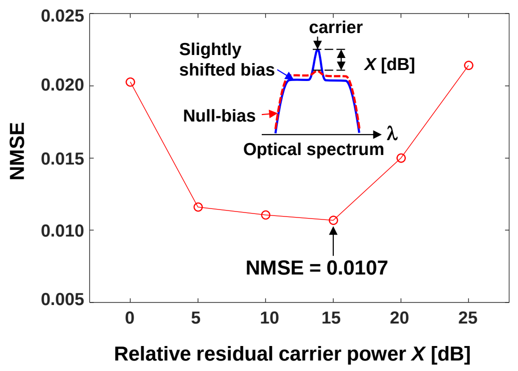

Fig. 3: Optimization of bias voltage. The definition of X is shown in the inset.

refresh rate 1/*T'* was 5.83 GHz. The modulated light was coupled to the RC chip through a lensed fibre with a spot size of ~2 μm. To thermally stabilize the speckle pattern measurement, we directly mounted the RC chip on the Peltier module with a resolution of 0.025 °C. The SMW-to-ring coupling ratio, *K*, was tuned by applying DC power to the heater via a probe.

The output light from the MMW was measured by scanning the position of the lensed fibre with a 0.5 μm step. Therefore, the total number of scanning points was 100. The light coupled to the lensed fibre and was then amplified by using an erbium-doped fibre amplifier (EDFA) and input to a photodiode (PD) after removing amplified spontaneous emission noise using an optical bandpass filter. The nonlinearity was provided by square-law PD detection. Finally, the electrical output from the PD was captured using a digital storage oscilloscope (DSO) operating at 80 Gsample/s. The digitized data were processed with an offline DSP consisting of frame synchronization, resampling, and temporal node decomposition. The training was performed using a linear regression. An example of the measured spatiotemporal evolution is shown in the inset of Fig. 2.

Results

We performed one-step ahead predictions using a Santa Fe time series as benchmark tasks [22]. The first 3000 points were used for training, and the following 1000 points were used for testing. All subsequent experimental results were obtained under the condition where the ring *K* was set to 0.2, being the optimum value derived by experiment. The NMSEs were averaged over three measurements for all results.

As a hyperparameter tuning, the NMSE was evaluated by changing DC bias V_{DC} of the intensity modulator [11,14]. In the experiment, V_{DC} was adjusted by measuring the residual carrier power in the optical spectrum of modulated light. Figure 3 shows NMSEs as a function of relative residual carrier power *X*, defined by carrier power deviation from null bias point (V_{DC} = 1.047 V) as shown in the inset of Fig.4. The minimum NMSE of 0.0107 was obtained for *X* = 15 dB, where V_{DC} = 1.113 V.

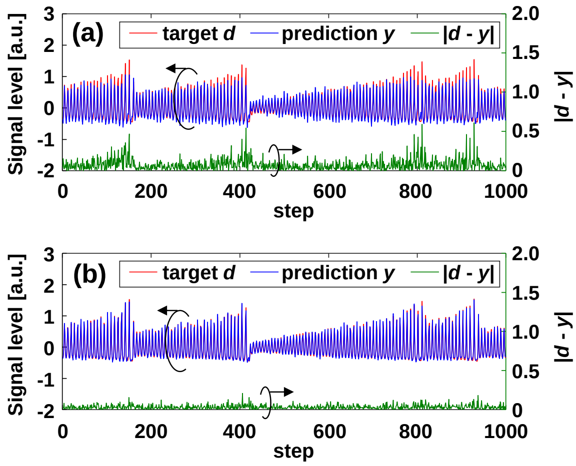

Fig. 4: Prediction result. (a) without MMI, NMSE = 0.0656, (b) with MMI, NMSE = 0.0107

We evaluated the NMSE with and without MMI-section for comparison. Figures 4(a) and (b) show the benchmark result for without and with MMI-section, and corresponding NMSE were 0.0656 and 0.0107, respectively. The prediction target *d*, the predicted result *y* and errors calculated from their difference |*d* - *y*| were shown. The prediction error |*d* - *y*| was suppressed more in Fig. 4(b) than in Fig. 4(a). The obtained NMSE of 0.0107 was smaller than the experimentally reported values by photonic RC, i.e., NMSEs of 0.02 [11], 0.016 [16] and 0.018 [19]. These results indicate that adding the MMW to the delayed feedback ring improved the prediction performance.

Conclusion

We have demonstrated a delay-based RC with MMI structure in a silicon photonic chip. By combining delayed feedback RC and MMI-based RC, the number of nodes was expanded to 1100. As a result, the NMSE for the Santa Fe time series one-step prediction task was greatly reduced to 0.0107.

References

[1] D. Amodei, D. Hernandez, "AI and compute," https://openai.com/research/ai-and-compute, 2018, accessed on 14 April 2023.

[2] M. A. Nahmias, B. J. Shastri, A. N. Tait, T.F.de Lima, and P. R. Prucnal, "Neuromorphic Photonics," *Optics & Photonics News*, vol. 29, no. 1, pp. 34-41, 2018, DOI: https://doi.org/10.1364/OPN.29.1.000034

[3] G. Van der Sande, D. Brunner, and M.C. Soriano, "Advances in photonic reservoir computing,"

Nanophotonics, vol. 6, no. 3, pp. 561-576, 2017, DOI: https://doi.org/10.1515/nanoph-2016-0132

[4] D. Brunner, B. Penkovsky, B. A. Marquez, M. Jacquot, I. Fischer, and L. Larger, “Tutorial: Photonic neural networks in delay systems,” *Journal of Applied Physics* vol. 124, no. 15, 152004, 2018, DOI: https://doi.org/10.1063/1.5042342

[5] M. Cucchi, S. Abreu, G. Ciccone, D. Brunner and H. Kleemann, “Hands-on reservoir computing: a tutorial for practical implementation,” *Neuromorphic Computing and Engineering*, vol. 2, 032002, 2022, DOI https://doi.org/10.1088/2634-4386/ac7db7

[6] Y. Paquot, J. Dambre, B. Schrauwen, M. Haelterman, and S. Massar “Reservoir computing: a photonic neural network for information processing”, in *Proceedings SPIE 7728*, *Nonlinear Optics and Applications IV*, 77280B, 2010, DOI: https://doi.org/10.1117/12.854050

[7] L. Appeltant, M.C. Soriano, G. Van der Sande, J. Danckaert, S. Massar, J. Dambre, B. Schrauwen, C.R. Mirasso and I. Fischer. “Information processing using a single dynamical node as complex system,” *Nature Communications,* vol. 2, 468, 2011, DOI: https://doi.org/10.1038/ncomms1476

[8] L. Larger, M. C. Soriano, D. Brunner, L. Appeltant, J. M. Gutierrez, L. Pesquera, C. R. Mirasso, and I. Fischer, “Photonic information processing beyond Turing: an optoelectronic implementation of reservoir computing,” *Optics Express*, vol. 20, no. 3, pp. 3241-3249, 2012, DOI: https://doi.org/10.1364/OE.20.003241

[9] Y. Paquot, F. Duport, A. Smerieri, J. Dambre, B. Schrauwen, M. Haelterman and S. Massar “Optoelectronic Reservoir Computing,” *Scientific Reports, v*ol. 2, 287, 2012, DOI: https://doi.org/10.1038/srep00287

[10] F. Duport, B. Schneider, A. Smerieri, M. Haelterman, and S. Massar, “All-optical reservoir computing,” *Optics Express,* vol. 20, no. 20, pp. 22783-22795, 2012, DOI: https://doi.org/10.1364/OE.20.022783

[11] M. C. Soriano, S. Ortín, D. Brunner, L. Larger, C. R. Mirasso, I. Fischer, and L. Pesquera, "Optoelectronic reservoir computing: tackling noise-induced performance degradation," *Optics Express,* vol. 21, no. 1, pp. 12-20, 2013, DOI: https://doi.org/10.1364/OE.21.000012

[12] K. Vandoorne, P. Mechet, T. Van Vaerenbergh, M. Fiers, G. Morthier, D. Verstraeten, B. Schrauwen, J. Dambre and P. Bienstman, “Experimental demonstration of reservoir computing on a silicon photonics chip,” *Nature Communications,* vol. 5, 3541, 2014, DOI: https://doi.org/10.1038/ncomms4541

[13] A. Dejonckheere, F. Duport, A. Smerieri, L. Fang, J. L. Oudar, M. Haelterman, and S. Massar, “All-optical reservoir computer based on saturation of absorption,” *Optics Express,* vol. 22, no. 9, pp. 10868-10881, 2014, DOI: https://doi.org/10.1364/OE.22.010868

[14] Q. Vinckier, F. Duport, A. Smerieri, K. Vandoorne, P. Bienstman, M. Haelterman, and S. Massar, “High-performance photonic reservoir computer based on a coherently driven passive cavity,” *Optica,* vol. 2, no. 5, pp. 438-446, 2015, DOI: https://doi.org/10.1364/OPTICA.2.000438

[15] L. Larger, A. Baylón-Fuentes, R. Martinenghi, V. S. Udaltsov, Y. K. Chembo, and M. Jacquot, “High-Speed Photonic Reservoir Computing Using a Time-Delay-Based Architecture: Million Words per Second Classification,” *Physical Review X*, vol. 7, 011015, 2017, DOI: https://doi.org/10.1103/PhysRevX.7.011015

[16] J. Vatin, D. Rontani, and M. Sciamanna, "Experimental reservoir computing using VCSEL polarization dynamics," *Optics Express*, vol. 27, no. 13, pp. 18579-18584, 2019, DOI: https://doi.org/10.1364/OE.27.018579

[17] M. Nakajima, K. Tanaka, and T. Hashimoto, “Scalable reservoir computing on coherent linear photonic processor,” *Communications Physics*, vol. 4, 20, 2021, DOI: https://doi.org/10.1038/s42005-021-00519-1

[18] M. Borghi, S. Biasi,and L. Pavesi, “Reservoir computing based on a silicon microring and time multiplexing for binary and analog operations,” *Scientific Reports,* vol. 11, 15642, 2021, DOI: https://doi.org/10.1038/s41598-021-94952-5

[19] S. Sunada and A. Uchida, “Photonic neural field on a silicon chip: large-scale, high-speed neuro-inspired computing and sensing,” *Optica*, vol. 8, no. 11, pp. 111388-1396, 2021, DOI: https://doi.org/10.1364/OPTICA.434918

[20] H. Tanaka, T. Kan, S. Ishimura, H. Takahashi, T. Tsuritani, K. Utaka, M. Suzuki, “Small-Footprint Photonic Reservoir Computing Chip Based on Speckle Patterns in a Multimode Waveguide,” in *Proceedings Conference on Lasers and Electro-Optics (CLEO2023*), San Jose, USA, 2023, paper SM1P.4.

[21] H. Takahashi, R. Inohara, K. Nishimura, and M. Usami, “Expansion of Bandwidth of Tunable Dispersion Compensator Based on Ring Resonators Utilizing Negative Group Delay,” *Journal of Lightwave Technology*, vol. 24, no. 6, pp. 2276-2286, 2006, DOI: https://doi.org/10.1109/JLT.2006.874588

[22] A. S. Weigend and N. A. Gershenfeld, “Results of the time series prediction competition at the Santa Fe Institute,” in *Proceedings IEEE International Conference on Neural Networks*, San Francisco, USA, 1993, pp. 1786-1793 vol. 3, DOI: https://doi.org/10.1109/ICNN.1993.298828